

## **Cathodic Protection System Applied to Steel Using Fiber Sheet and Al-based Alloy Anode in Atmospheric Environment**

Muye Yang<sup>1</sup>, Shigenobu Kainuma<sup>1,\*</sup>, Shusen Zhuang<sup>1</sup>, Shuji Ishihara<sup>2</sup>, Akira Kaneko<sup>3</sup>, and Takao Yamauchi<sup>4</sup>

<sup>1</sup> Department of Civil Engineering, Faculty of Engineering, Kyushu University, Fukuoka 8190395, Japan

<sup>2</sup> Research & Development Hq. Tamano Technology Center, Mitsui Engineering & Shipbuilding Co., Ltd. Tamano 706-0014, Japan

<sup>3</sup> Surface Innovation Group, Nikkei Research & Development Center, Nippon Light Metal Company Ltd., Shizuoka 421-3291, Japan

<sup>4</sup> Production Division, Saidaiji Plant, Japan Exlan Co., Ltd., Okayama 704-8194, Japan

\*E-mail: [kai@doc.kyushu-u.ac.jp](mailto:kai@doc.kyushu-u.ac.jp)

*Received:* 31 May 2019 / *Accepted:* 2 July 2019 / *Published:* 30 August 2019

---

In this study, we developed a cathodic protection (CP) system, which includes a sacrificial anode and a moisture-absorbent fiber sheet, and applied it to old steel structures exposed in a chloride environment, especially localized steel members susceptible to corrosion. Additionally, we evaluated the effects of environmental changes caused by the electrolyte and anodic material on the durability and effectiveness of the CP system. To verify the corrosion kinetics of steel affected by the sacrificial anode, electrochemical tests on binary and ternary alloys were conducted in an immersion environment and the corresponding electrochemical tests on specimens with CP were conducted in an indoor atmospheric environment. Moreover, the anti-corrosion mechanism and time-dependent current variations were clarified by conducting exposure corrosion tests. The test results demonstrated that the anodic reaction kinetics of Al-3Zn and Al-20Zn were similar; Al-based alloy could be a sacrificial anode with a stable activating reaction, providing sustained CP for steel through an aquiferous fiber sheet. Furthermore, the fiber sheet acted as an effective electrolyte in the atmospheric environment and led to a sustained anti-corrosion current and negative potential at the steel member. In addition, high chloride or nonuniform electrolyte was considered the reason for the occurrence of self-corrosion in a steel plate, which can be avoided by adjusting the dimensions of the exposed holes in the anode plate.

---

**Keywords:** steel structure; atmospheric corrosion; passive cathodic protection; Al-based alloy; electrochemical test

## 1. INTRODUCTION

The degradation of coating films of steel structures in use mainly results from hydrolysis and oxidative decomposition [1,2], further exposing the steel to the environment. Besides coatings, cathodic protection (CP) is the most common method used for protecting structures from corrosion in a marine environment [3,4]. Today, many ships and offshore platforms are protected from corrosion by an electrical method of sacrificial anode cathodic protection (SACP). The main practical use of SACP is to protect steel structures buried in soil or immersed in water. In principle, SACP systems can be applied to any metallic structure in contact with an electrolyte, but its current application in an atmospheric environment is still rare and incurs issues. Mostly because of the complex and multiple environmental changes, only limited humidity can be provided by the atmospheric environment, from rainfall and dew.

Thus far, several atmospheric corrosion kinetics of mild steel that may be involved are attract considerable attention in laboratory and in-site tests [1,5–7]. Some effective CP techniques have been developed for the reinforced concrete structures in service [8]. Some scholars have also recommended the application of the CP technique to new steel structures, such as using submerged sacrificial anodes for preventing the atmospheric exposed part of marine structures [9,10]. However, for aging steel structures exposed in an aggressive atmospheric environment, such as the girder web or pile bottom of steel bridges, which are susceptible to corrosion, an effective CP method is difficult to apply in practice. Not only the complicated atmospheric corrosion kinetics of mild steel but also specific environmental factors, such as salt concentration, wet–dry cycles, and temperature changes, particularly the characteristics of the cathode metal itself, such as the rough surface condition or residual rusts, affect the durability and effectiveness of a passive CP system.

In practice, the electrochemical properties of various anode materials have a significant influence on system effectiveness. The current efficiency of sacrificial anode materials, in terms of factors, such as hardness, durability, and cost, have also become influential parameters for considering specific in-site applications [10–14]. At present, Al anodes are favored over Zn anodes for the CP of offshore structures, because they are lighter, less expensive, and exhibit larger current capacity [15,16]. Additionally, to lower the potential of anode alloys, zinc, and indium are the most commonly used modifiers [12,17,18]. Salinas et al. discussed the electrochemical behavior of Al-Zn alloys with various Zn contents in a 0.5 wt% sodium chloride solution [19]. Previous research has suggested that the Al-Zn-In series of sacrificial anodes exhibits superior characteristics, especially for seawater applications [20]. However, these laboratory test results focused on electrochemical properties of anode alloys in the short term, without actually considering the time-dependent effects.

Previously, CP was developed to be applied to actual steel members in an atmospheric environment, which is susceptible to local corrosion [21–24]. This protection system includes a sacrificial anode and a moisture-absorbent fiber sheet acting as the electrolyte carrier. The present study aims to determine the influence of environmental changes caused by the electrolyte and anodic material on the durability and effectiveness of the CP system. Herein, three types of Al alloys are used as the anode, and their electrochemical properties are demonstrated through corrosion potential, polarization curve, and galvanic coupling current of the samples immersed in different concentrations of NaCl aqueous solutions. Additionally, to verify the sustained negative potential shift and corrosion kinetics of steel

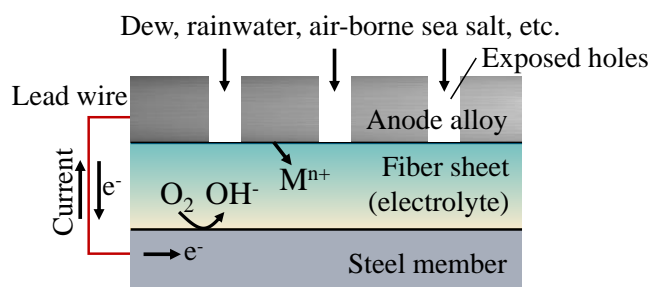
affected by different anode alloys and solution concentrations, corresponding electrochemical tests on specimens with CP are conducted in an indoor atmospheric environment. Furthermore, two exposure corrosion tests are conducted in a thermo-hygrostat, to determine the durability of the CP system using different anode materials and the differential aeration corrosion caused by the exposed holes.

## 2. EXPERIMENTAL

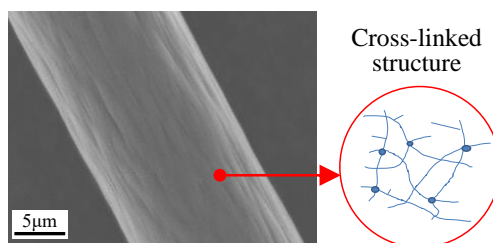
### 2.1. Method and materials

The CP system used in this study includes a fiber sheet (electrolyte carrier) and an Al-based casting alloy (sacrificial anodic material), which are fixed together and attached to a surface-cleaned steel member (cathodic material). The steel member directly fays with the fiber sheet, and is connected to the anode metal by lead wires. The fiber sheet acts as the electrolyte carrier, which implies that the aquiferous fiber sheet between the two types of metals acts as the electrolyte for sustaining the ion flow between the anode and cathode, so that an electric circuit can be established, as illustrated in Fig. 1.

Two types of binary alloys, Al-3Zn and Al-20Zn (wt%), and one ternary alloy, Al-3Zn-0.02In (wt%), are cast as the anodic metal; their chemical compositions are listed in Table 1. The chemical compositions of the mild steel used in the electrochemical test and indoor exposure test are listed in Table 2.



**Figure 1.** Schematic of the CP system and its electric circuit between cathodic steel member and anodic alloy plate.



**Figure 2.** Microscopy photographs of dry cross-linked acrylate fiber.

**Table 1.** Chemical compositions of the anode alloy plate used as anodic material in the CP system.

Anode alloy	Chemical compositions (wt%)			Dimension of alloy samples (mm)	Dimension of alloy plate used in specimen (mm)
	Al	Zn	In		
Al-3Zn	97	3	-	33 × 5 × 5	66 × 66 × 5

Al-20Zn	80	20	-
Al-3Zn-0.02In	96.98	3	0.02

**Table 2.** Chemical compositions of the mild steel used as a cathodic material in the CP system.

Specification of steel material	Chemical compositions (wt%)							
	C	Si	Mn	P	S	Cu	Ni	Cr
JIS G 3106 SM490A	0.16	0.14	0.69	0.013	0.004	0.01	0.02	0.02

Additionally, the water absorption properties of the fiber sheets are strongly related to the effectiveness of the system. Herein, an acrylate fiber mixed with 70% cross-linked acrylate fiber and 30% polyester fiber is used for testing; the microscopy photograph of the dry cross-linked acrylate fiber is shown in Fig. 2. The structure of the cross-linked acrylate fiber is formed by the bonding of fibers, providing voids for absorbing water. Osmotic pressure is the main kinetics for the water absorption of such a fiber. The test results of a previous study showed that the moisture absorptivity of the fiber sheet has a rough direct relation with environmental relative humidity [25].

## 2.2. Electrochemical test

### (1) Test samples

Anodic alloy samples ( $33 \times 5 \times 5 \text{ mm}^3$ ) and mild steel samples ( $33 \times 7 \times 5 \text{ mm}^3$ ) were manufactured. The cut surfaces were polished using abrasive paper (#600 and #1000) to make the entire surface flat and uniform. Electrochemical tests on the samples were conducted in an immersion environment at room temperature (20 °C). Here, 0.1 wt% simulated rainwater, 3.5 wt% simulated seawater, and saturated 26.4 wt% NaCl solutions were used as the electrolytes. All electrolytes used in this study were prepared from ion-exchanged water. During the test, the distance between the two samples in the NaCl aq solution was set as 30 mm.

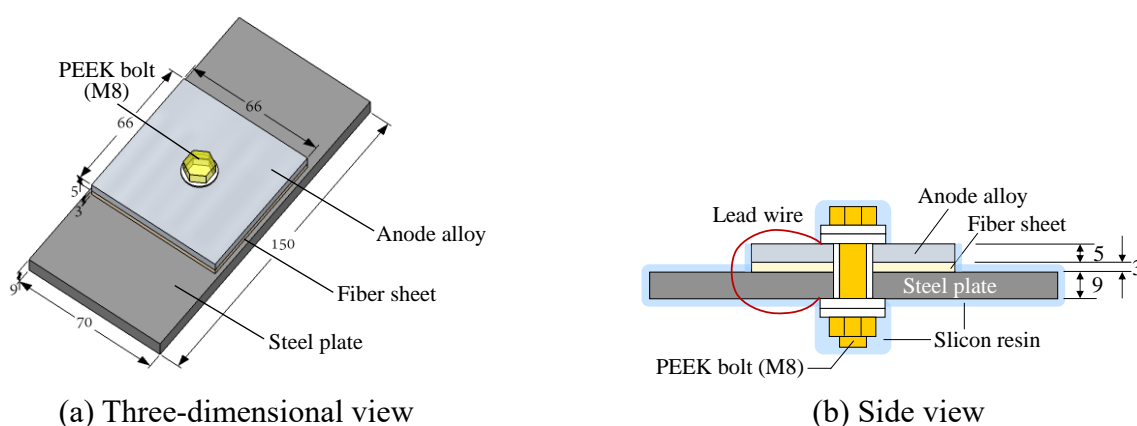
The corrosion potentials ( $E_{\text{corr}}$ ) of the three types of alloy samples were measured for 1800 s when an Ag/AgCl electrode in saturated potassium chloride (Sat.KCl) solution was used as the reference electrode. After reaching a stable potential value, a platinum sheet plate was additionally used as a counter-electrode for the polarization measurement. A typical anodic polarization scan was started at  $-0.1 \text{ V vs. } E_{\text{corr}}$  to  $+0.5 \text{ V vs. } E_{\text{corr}}$ , with a scan rate of 20 mV/min [26]. Then, three alloy samples under the 0.1 wt% NaCl aq solution and one Al-3Zn sample under different concentrations of 0.1, 3.5, and 26.4 wt% NaCl aq solution were scanned. Furthermore, the galvanic coupling currents between the steel sample and the three types of anodic alloy samples were measured using a zero-resistance ammeter, in intervals of 10 min.

### (2) Test specimens

The test specimens included a mild steel plate ( $150 \times 70 \times 9 \text{ mm}^3$ ), an aquiferous fiber sheet ( $66 \times 66 \times 3 \text{ mm}^3$ ), and an anode alloy plate ( $66 \times 66 \times 5 \text{ mm}^3$ ). The influences of the three types of anode alloys (Al-3Zn, Al-20Zn, and Al-3Zn-0.02In) were also compared when they acted as a sacrificial anode

for the CP system in the atmospheric environment. In the anode alloy plate, eight circular holes with a diameter of  $\phi = 6.5$  mm were set as exposing holes, so that the moisture from the exterior of the specimen could be quickly absorbed by the fiber sheet in an atmospheric environment. The components of the CP system were fixed using a polyetheretherketone (PEEK) bolt at the center hole ( $\phi = 10$  mm) and tightened with a torque of  $\sim 3$  N·m. A lead wire was connected with cathode and anode metals to maintain a short circuit in the system. The specimens were the same as those depicted in Fig. 3.

Electrochemical tests on the specimens were conducted in an atmospheric environment at room temperature (20 °C). NaCl solutions with concentrations of 0.1, 3.5, and 26.4 wt% were absorbed sufficiently by the fiber sheet in advance, so that the aquiferous fiber sheet could be used as an electrolyte during the tests. The galvanic potential and polarization scan of the steel plate in the CP specimens were measured using the same methods as those described previously (see electrochemical test on samples). During anodic polarization scanning, only the Al-3Zn alloy was used as the sacrificial anode.



**Figure 3.** Dimensions and components of the specimen with CP system (unit: mm).

### 2.3. Constant exposure corrosion test

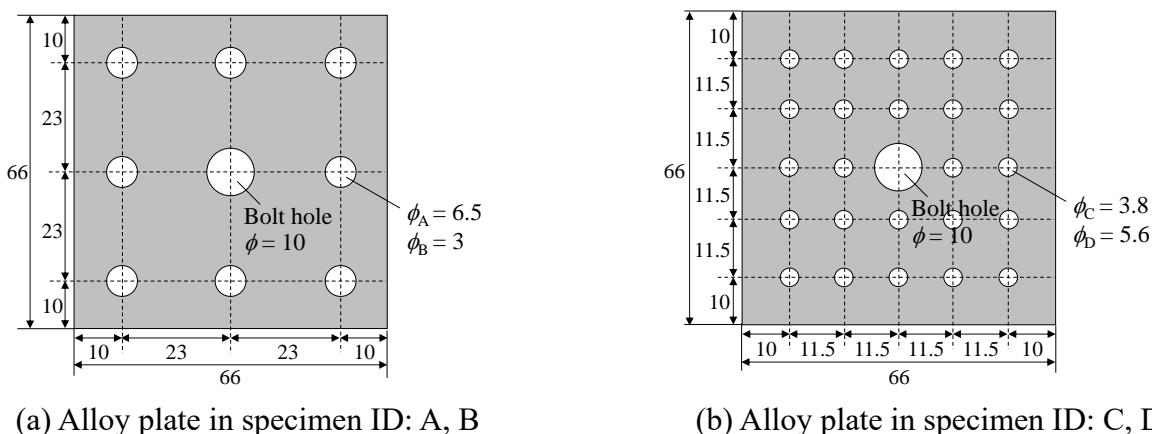
#### (1) Durability of the CP system using different anode materials

This section shows the indoor exposure corrosion test performed in a constant environment to investigate the effect of the anode material and area of the exposed holes on anti-corrosion effectiveness. The exposure corrosion test was conducted in a thermo-hygrostat. Three specimens with different anodic alloy plates (Al-3Zn, Al-20Zn, and Al-3Zn-0.02In) were tested horizontally in the following constant environment, which was controlled at a constant temperature of 30 °C and relative humidity (RH) of 100%. The initial electrolyte absorbed by the fiber sheet used 26.4 mass% NaCl aq, so that the sacrificial anodic protection effect could be easily exhibited. The galvanic current of the entire constant exposure test was recorded by a zero-resistance ammeter every 10 min for 780 h.

#### (2) Differential aeration corrosion caused by exposed holes

The specimens with four types of exposed holes in the Al-3Zn alloy plate were tested horizontally by corrosion exposure in a thermo-hygrostat, with a constant temperature of 50 °C and an RH of 35%.

When the measured current was dropped to approximately zero, the fiber sheet was fed manually with distilled water, and this operation was conducted four times during a 300 h constant exposure test.



**Figure 4.** Arrangement and numbers of exposed holes in Al-3Zn alloy plate used in the constant exposure corrosion test (unit: mm).

**Table 3.** Diameters of exposed holes of four alloy plates used in the constant exposure corrosion test.

Specimen ID	Dimensions of exposed holes in alloy plate		Exposed hole area (mm <sup>2</sup> )	Exposed hole type
	Diameter (mm)	Total number		
(A)	$\Phi$ 6.5	8	$33.2 \times 8 = 265.6$	Standard
(B)	$\Phi$ 3	8	$7.1 \times 8 = 56.8$	Small-hole type
(C)	$\Phi$ 3.8	24	$11.3 \times 24 = 271.2$	Multi-hole type
(D)	$\Phi$ 5.6	24	$24.6 \times 24 = 590.4$	Multi-hole type

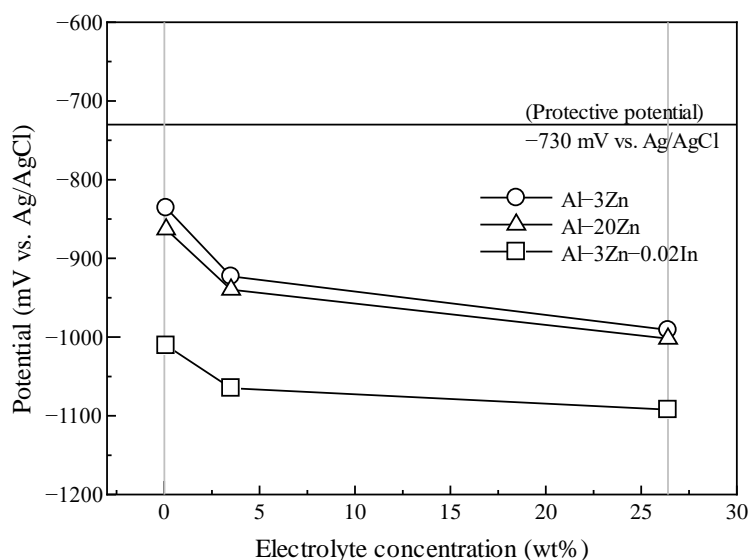
Four types of exposed holes in the anode alloy plate were drilled with different diameters and total areas, and the corresponding specimens were denoted as (A), (B), (C), and (D), as listed in Table 3. Samples (A) and (B), and (C) and (D), had holes of the same arrangement and numbers, with different diameter, as shown in Fig. 4. The exposed holes of sample (A) were set as the standard type, exactly the same as those of the specimens tested in previous tests. The total area of the circular air holes in this alloy plate was approximately 6% of the residual surface area, excluding the bolt hole area, which was calculated according to Archimedes' principle (JIS R 2205) [27]. The holes of sample (B) was set as a small-hole type with a smaller diameter and total area of exposed holes. Those of sample (C) were set as a small/multi-hole type, having approximately the same exposed area as that of the standard type (A) with a smaller diameter and a large number of exposed holes. The holes of sample (D) were set as a multi-hole type, with the largest total exposed area and a large number of holes.

### 3. RESULTS AND DISCUSSION

#### 3.1. Electrochemical characteristics of anode alloy

The corrosion potentials of the three types of anodic alloy samples demonstrated that all of them tended to be more negative as the concentration of NaCl aq was increased from 0.1 wt% to saturated 26.4 wt%, regardless of the composition, as shown in Fig. 5. The measured potentials of Al-Zn binary alloys were varied between 140 mV and 155 mV, while the potential variation of ternary alloy Al-3Zn-0.02In was about 80 mV when the concentration was varied from 0.1 to 26.4 wt%. Additionally, there was no significant change in the self-potential of Al-Zn binary alloy when the additive amount of Zn was between 3 and 20%. Their sensitivity to  $\text{Cl}^-$  concentration was also similar.

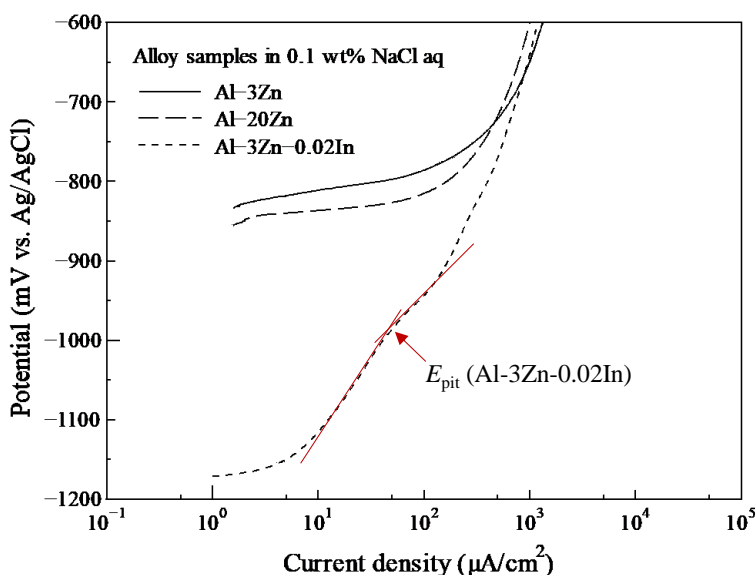
The potential of commercial Al-Zn-In alloys has been widely reported to be around  $-1.1$  V in different chloride media. At present, Al-Zn-In is widely known to exhibit the best performance in seawater [28,29]. In this study, the addition of 0.02 wt% In, of the total weight, led to a large negative shift in potential, the potential gap between the ternary alloy and Al obtained in the test result consistent with the finding of Fagbayi et al., where In typically shifted the spontaneous potential of Al by 0.3 to 0.5 V in the negative direction [15]. Therefore, the additional In element had an evident influence on the electrochemical test results, where Al-3Zn-0.02In exhibited the most negative self-potential.



**Figure 5.** Corrosion potential of three alloy samples when immersed in 0.1, 3.5, and saturated 26.4 wt% NaCl aq.

Fig. 6 shows the anodic polarization curves of the three alloy samples in 0.1 wt% NaCl aq, where the passivation inhibition of the alloy occurs in all samples. Therefore, the activating reaction of alloy corrosion indicates the occurrence of a uniform dissolution in a neutral chloride ionic solution when alloy works as a sacrificial anode. Additionally, the anodic polarization curves of all three alloy samples present a weak polarization zone and a Tafel zone regardless of the chemical compositions, but the distribution shows a different tendency between the binary and ternary alloys. For binary alloy samples,

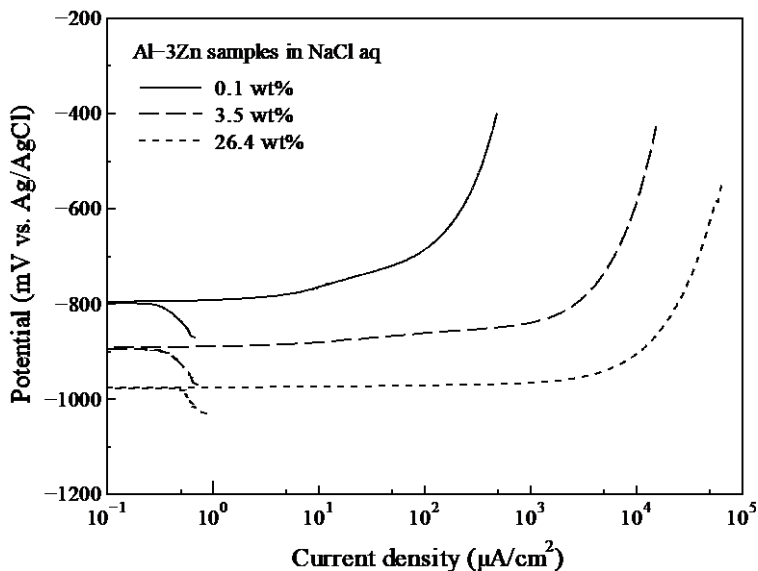
more proportion of Zinc would cause a slight decrease in potential and a slight increase in corrosion current, whereas the polarization characteristic indicates that their Tafel constants ( $\beta_a$ ) and exchange current densities are approximate. In other words, the anodic reaction kinetics of Al-3Zn and Al-20Zn are expected to be the same. For the ternary alloy Al-3Zn-0.02In, its self-potential would be shifted to a more negative direction due to the additional In element. Additionally, the pitting potential appears in the polarization curve, but its dissolution continues with an increase in the overpotential. Moreover, it has a smaller exchange current density than that exhibited by the binary alloy Al-Zn, which leads to a higher current efficiency. Above all, the activator elements (Zn and In) ensure a uniform dissolution of the anodic metal and enhance the dissolution kinetics in the NaCl aq environment [30].



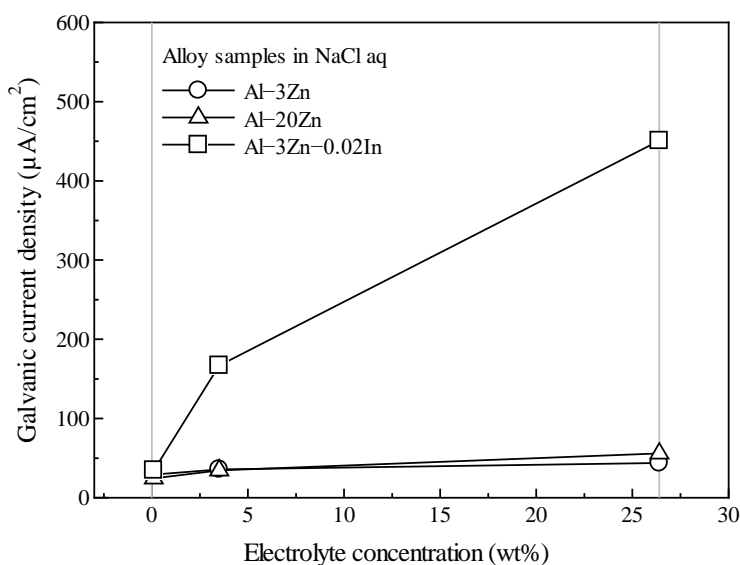
**Figure 6.** Anodic polarization curves of three alloy samples when immersed in 0.1 wt% NaCl aq.

For the NaCl aq electrolyte of different concentrations, the polarization curves of Al-3Zn samples display similar distributions, as shown in Fig. 7. There is no evident pitting potential in any case, which indicates that Al-3Zn is a sacrificial anode with a stable activating reaction regardless of the electrolyte concentration. However, the weak polarization zone of Al-3Zn shows the difference in various concentrated NaCl aq solutions, and thus, both the potential and exchange current density of the anode metal would be changed according to the environmental salinity. Its self-potential would be shifted to a more negative direction in the range of 200 mV, according to a higher concentration of the electrolyte. Additionally, the corrosion current density increases rapidly when the anodic overpotential slightly deviates in the highly concentrated electrolyte, which indicates that the anodic dissolution tends to be easier under the high-Cl<sup>-</sup>-concentration solution. This phenomenon shows that the CP system can accommodate to the aggressive environment with salt accumulation.





**Figure 7.** Anodic polarization curves of Al-3Zn samples when immersed in 0.1, 3.5, and saturated 26.4 wt% NaCl aq.



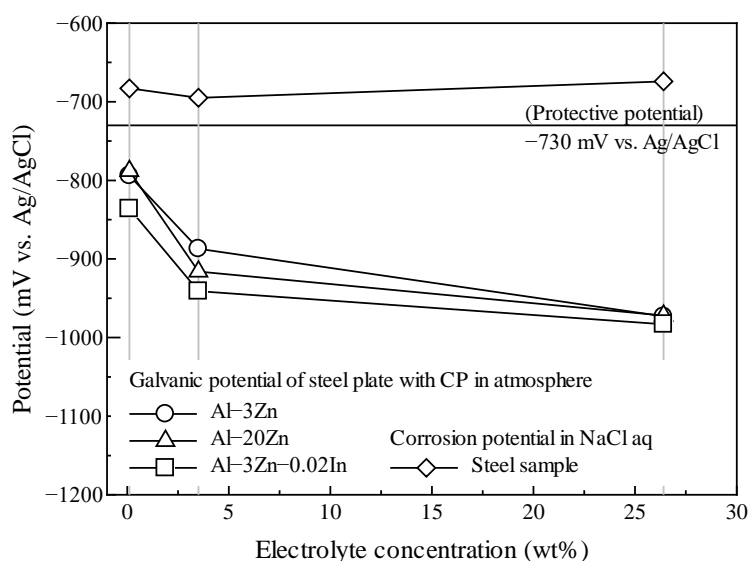
**Figure 8.** Galvanic coupling current density between the three types of anodic alloy samples and a steel sample in 0.1, 3.5, and 26.4 wt% NaCl aq.

The galvanic coupling currents between the steel and alloy samples were measured in an immersion environment of NaCl aq solution. The calculated current densities in 0.1, 3.5, and 26.4 wt% NaCl aq are shown in Fig. 8. Obviously, they tend to increase with the electrolyte concentration. The Al-3Zn and Al-20Zn alloy samples present similar galvanic coupling current densities. The increase in the proportion of Zn does not play a significant role in promoting the anti-corrosion efficiency. Meanwhile, when the steel sample is galvanized with the Al-3Zn-0.02In sample, its current density is largely enhanced by the increase in the electrolyte concentration. Compared to the current densities of the Al-Zn binary alloy in 3.5 wt% NaCl aq, that of Al-3Zn-0.02In is approximately five times larger.

However, under the immersion environment of a high-Cl<sup>-</sup>-concentration solution, Al-3Zn-0.02In provides an oversized anti-corrosion current density when it acts as a sacrificial anode, which is more than 10 times the current density required for electrochemical corrosion protection in seawater, which is suggested to be  $\sim 10 \mu\text{A}/\text{cm}^2$  by Ishihara [31].

### 3.2. Passive cathodic characteristics in the CP system

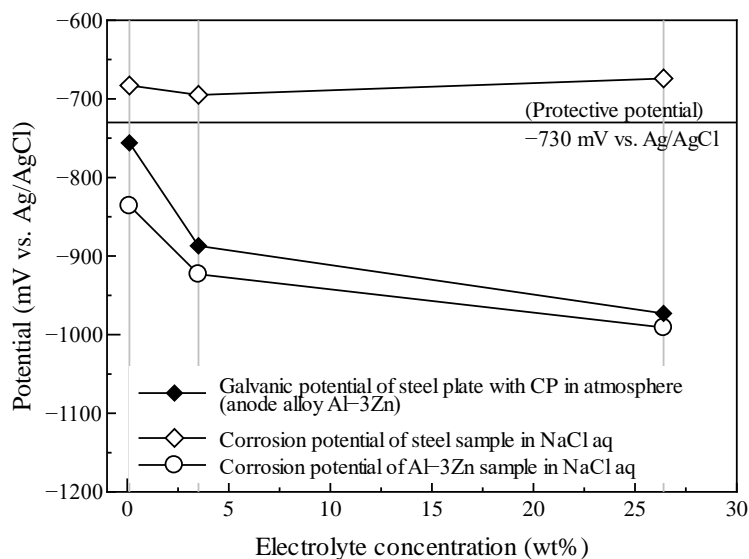
Fig. 9 shows the galvanic potential of the steel plate in specimens affected by the three types of alloys for the specimens with CP system (Fig. 3) exposed in the atmospheric environment. It also shows that the corrosion potential of steel without anodic protection is approximately -675 to -695 mV and that the correlation between the potential of steel and Cl<sup>-</sup> concentration is not significant. In general, the protective potential of steel members in a neutral environment is approximately -730 mV vs. Ag/AgCl [32]; herein, the passive galvanic potentials of cathodic steel in all three specimens is met the requirements and exceeds the effective protective potential.



**Figure 9.** Comparison of galvanic potential of steel affected by three types of anode alloys under different electrolyte concentrations.

Note that when the alloy plate is coupled with a steel plate through an aquiferous fiber sheet in an atmospheric environment, the galvanic potential of the specimen affected by the different types of anode alloys shows roughly the same potential shift. In case of the fiber sheet with 0.1 wt% NaCl aq electrolyte, the negative shift on the passive galvanic potential of the steel is  $\sim 105$ – $111$  mV when Al-Zn acts as the anode; this value is  $\sim 153$  mV when Al-3Zn-0.02In acts as the anode. In case of the fiber sheet with 26.4 wt% NaCl aq electrolyte, all three anodes can lead to a negative shift of  $\sim 300$  mV on the galvanic potential of steel, and the induced negative potentials (below -970 mV vs. Ag/AgCl) are sustained in a constant environment.

The stable potentials of steel and Al-3Zn samples in NaCl aq solutions are used to compare the passive galvanic potential of the steel plate in the specimen with Al-3Zn and the aquiferous fiber sheet in the CP system, as shown in Fig. 10. Obviously, when the alloy plate is coupled with the steel plate through the aquiferous fiber sheet, the alloy plate acts as the sacrificial anode and induces a significant negative deflection in the potential of steel. In addition, the passive galvanic potential of the steel plate tends to be more negative as the Cl<sup>-</sup> concentration of NaCl aq absorbed by the fiber sheet, in advance, is increased from 0.1 to 26.4 wt%. This result is consistent with the measured potential of Al-3Zn sample in an immersion environment.



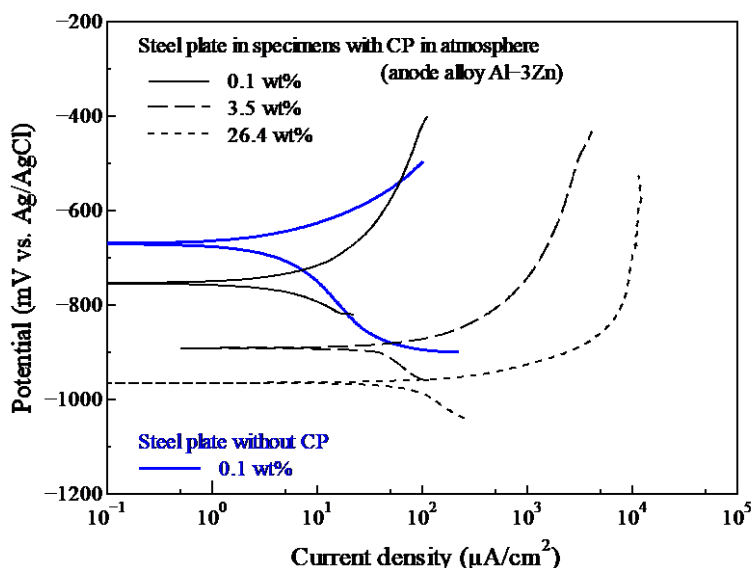
**Figure 10.** Comparison of potential and galvanic potentials of steel under the different electrolyte concentrations.

Particularly, when a fiber sheet acts as an electrolyte carrier and the NaCl aq inside acts as an electrolyte, the coupling potential of the steel plate is very close to the corrosion potential of Al-3Zn, regardless of the solution concentration. It is indicated that the aquiferous fiber sheet can be a stable electrolyte in the atmospheric environment and lead to a stable passive shifting in the galvanic potential at the steel surface, because of its special cross-linked structure with a hydrophilizing functional group. Additionally, a previous study [33] clarified that the resistance of an aquiferous fiber sheet can be ignored, while its electric conductivity and ion diffusion are slightly different from those of the aqueous electrolyte, which would cause the reduced effectiveness on a large time scale.

The polarization curves of the steel plate affected by anode alloy Al-3Zn, for the specimens with CP exposed in an atmospheric environment, are shown in Fig. 11. The polarization curves of the steel plate without CP in NaCl aq are also measured. The test result shows that the exchange current densities of steel with and without CP are approximate under the same environmental concentration, whereas the difference in the corrosion potentials equals to ~85 mV. Moreover, their Tafel slopes differ in the linear high-field region, which is a kinetic parameter of corrosion and determines the reaction process. A steel

plate with sacrificial anode affection has a smaller Tafel constant ( $\beta_a$ ), which indicates that the same overpotential leads to a smaller current density (corrosion rate) compared to the case without CP.

In addition, for the three specimens, both the shifted potential and exchange current density increase with the electrolyte concentration. Furthermore, the exchange current densities of the steel are smaller than those of binary alloy and close to that of Al-3Zn-0.02In alloy in the low-concentration electrolyte. Although self-corrosion might exist for steel in the high-Cl<sup>-</sup>-concentration environment, the active anodic dissolution of Al-3Zn can provide enough anti-corrosion current density continuously.



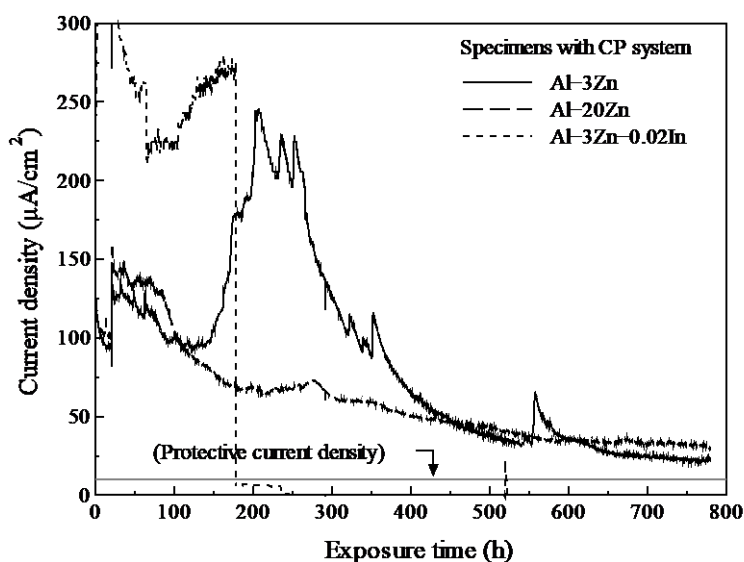
**Figure 11.** Polarization curves of steel plate measured at the different electrolyte concentrations.

### 3.3. Constant exposure test results

The sustained stable negative potential of steel occurs in a constant internal environment where the internal conditions of the fiber sheet and related contact status do not change with time. In this study, a thermo-hygrostat can only provide a stable external environment with constant temperature and RH. During the constant exposure test duration of 780 h, the water content in the fiber sheet changes with time, which leads to changes in the internal environment. In this study, the water content in the fiber sheet cannot be accurately measured during the exposure test, and the water content distribution inside the fiber sheet might also be in disequilibrium. Therefore, the time-dependent variation in water content inside the fiber sheet is not discussed in this paper, and instead, the influence of the fiber sheet states can be reflected in the current values and corrosion products.

The galvanic current density variations of the three specimens with different anode Al-3Zn are shown in Fig. 12. The initial current densities of Al-3Zn-0.02In specimen are much larger than those of the other two specimens. Its initial current density exceeds  $300 \mu\text{A}/\text{cm}^2$ , which is about 30 times larger than the current density required for electrochemical CP in seawater ( $10 \mu\text{A}/\text{cm}^2$ ) [31]. However, after 178 h, the current of specimen Al-3Zn-0.02In rapidly drops to zero. This abnormal condition indicates that the relation between electrochemical properties and anti-corrosion effect of sacrificial anode is more

complex in this system, because of the specific applied environment. Al-3Zn-0.02In alloy has great anti-corrosion characteristics such as high current efficiency, low self-corrosion rate, and more negative potential; however, the Al-3Zn-0.02In specimen with the CP system does not show advantages of durability. On the contrary, the time-dependent current density of Al-3Zn-0.02In specimen shows an extreme instability. Presumably, the electrolyte contained by the fiber sheet is different from the aqueous environment. The component contact situation is also influenced by factors such as volume shrinkage of the fiber sheet and deposition of corrosion products. The open circuit of Al-3Zn-0.02In specimen is attributable to these reasons.



**Figure 12.** Galvanic current density between alloy and steel plate when the fiber sheet contains 26.4 wt% NaCl aq electrolyte (30 °C, RH 100%).

The other two specimens with anodic binary alloy Al-Zn can obtain a sustainable corrosion protection effect. After 400 h of testing, the galvanized current densities tend to be below 50  $\mu\text{A}/\text{cm}^2$ . From 700 to 780 h, the galvanic current density reaches stable values with slight fluctuations. Among them, the Al-20Zn specimen has the most stable gradient change in the current density. As mentioned before, the galvanic potential of the specimen affected by the different types of anode alloys shows roughly the same potential shift (Fig. 9), and Al-3Zn-0.02In can provide an overlarge current density in a short term, while binary Al-Zn anode can provide a sustained CP for steel through an aquiferous fiber sheet in a moisture environment. A previous observation of the ternary alloy was that it shows much better electrochemical properties than Al-Zn alloy (Figs. 5 and 6). However, during the previous field exposure test [33] and constant exposure test, the ternary alloy Al-Zn-In did not show any advantage in terms of both durability and anti-corrosion effectiveness [34]. The electrolyte environment provided by the fiber sheet might limit the advantage of Al-Zn-In in wet-dry cycles.

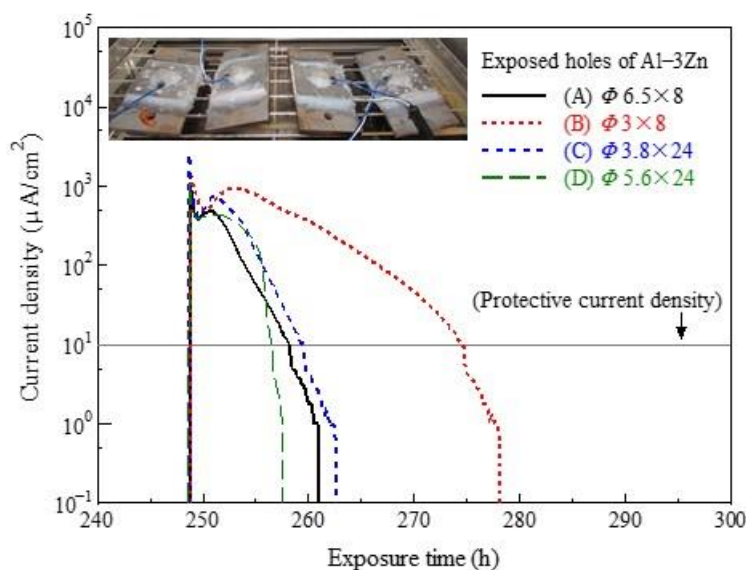
The current surges appear in Al-3Zn specimen after 200 h of testing, and then reduce back to the normal value. The test results indicate that the electrochemical properties of Al-3Zn and Al-20Zn are

similar, and thus, the difference in their current variation is not only caused by these two anode alloys but also by the electrolyte distribution inside the fiber sheet. Because the CP system aims to apply the steel structure in the atmospheric environment, the actual wet–dry cycles might cause a nonuniform electrolyte distribution inside the fiber sheet, and then lead to differential aeration corrosion or a decline in durability. This can be improved by adjusting the dimensions of the exposed holes.

### 3.4. Differential aeration corrosion caused by exposed holes

In an atmospheric environment with high temperature and humidity, a differential aeration corrosion might occur in steel plates in the vicinity of the exposed holes. In this system, the differential aeration corrosion can be caused by different environmental factors such as difference in dryness of the fiber sheet, partial temperature rises in metal, exposed area ratio between the cathode and anode parts, and interspace air access between the fiber and metal. Some impact factors can be controlled to suppress the differential aeration corrosion, by reducing the diameter or number of exposed holes. Simultaneously, some other impact factors can also have a negative influence.


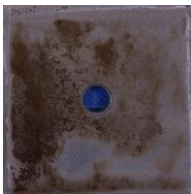
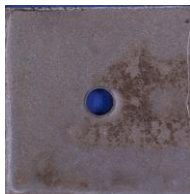
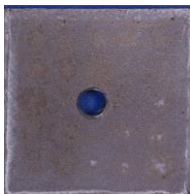


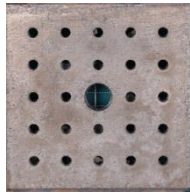
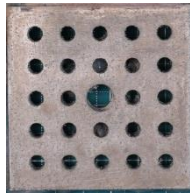
The current changes caused by the water supply are always similar; therefore, Fig. 13 only displays the current density variation after the fourth water supply, ~240–300 h after the test starts. The responses of the current densities caused by water supply are similar in different specimens, and the current densities are immediately restored for a value larger than  $1,000 \mu\text{A}/\text{cm}^2$ . Therefore, there is no difference in the responses of the anti-corrosion current caused by rainfall in real-life environments. However, the magnitude of the area of the anode material matches the anti-corrosion current value. With passage of the test time, the reduction speed of the current density demonstrates that  $(D) > (A) \approx (C) > (B)$ . Therefore, the area of the exposed holes directly determines the effective CP time. The single-side area of the alloy plate around the exposed hole area is inversely proportional to the effective operating time in this system.



**Figure 13.** Galvanic current density between alloy and steel plate in four types of specimens (Al-3Zn, 50 °C, RH 35%).

The surface conditions of four steel and alloy plates after 300 h of testing are presented in Table 4. On the steel surfaces of samples (A) and (D), slight corrosion can be observed on the periphery of the corresponding position of the exposed holes. This is the initial state of the differential aeration corrosion, easily formed in steel plates in the vicinity of the exposed holes, particularly for holes with a large diameter. Comparing the time-dependent current densities and tested steel surfaces of samples (A) and (D), the anode with the multi-hole type (D) does not provide a better effect than that with the standard type (A) on CP.

**Table 4.** Surface conditions of four specimens after 300 h of exposure corrosion test (Al-3Zn, 50 °C, RH 35%).

	(A) $\phi 6.5 \times 8$	(B) $\phi 3 \times 8$	(C) $\phi 3.8 \times 24$	(D) $\phi 5.6 \times 24$
Steel plate				
Al-3Zn alloy plate				

However, it is undetermined if the corrosion at the steel surface of samples (B) and (C) is caused by the differential aeration corrosion. In these cases, the diameter of the exposed holes is relatively small, particularly for the anode type (B) having a very small total exposed area, leading to a black corrosion product of steel. This result is attributable to the semi-dry state of the fiber sheet, due to the nonuniform evaporation of the electrolyte inside the fiber sheet. The small diameter of the holes usually lead to less water evaporation in the fiber sheet. Specifically, one side of the fiber sheet dries in the presence of contacts with the alloy plate, whereas another side remains wet in the presence of contacts with the steel plate. In this case, the fiber sheet loses its function as an electrolyte and its semi-dry state can cause self-corrosion of the steel plate.

Therefore, by adjusting the dimension of the exposed holes, the small exposed hole can lead to a nonuniform evaporation of the electrolyte in the fiber sheet and the semi-dry state of the fiber sheet is likely to cause self-corrosion of the steel plate. Additionally, it has been confirmed that the area of the exposed holes directly determines the effective CP time, while the number of holes has little influence on the anti-corrosion performance of the steel member. Above all, the standard type (A) is suitable for a

CP system, although it is under the risk of differential aeration corrosion, which requires further investigation.

#### 4. CONCLUSIONS

A CP system was developed for application to the steel members in an atmospheric environment. This study mainly discussed the material properties of components in this system and the anodic performance of three types of Al alloys. The electrochemical tests and constant exposure corrosion tests were conducted on specimens with CP to clarify the anti-corrosion mechanism and durability.

1) Electrochemical studies on the anodic alloy samples were performed in NaCl solutions of various concentrations. The galvanic characteristics of Al-3Zn-0.02In were the most satisfactory among the three types of alloy materials in solution. It has a more negative self-potential and smaller exchange current density than binary alloy Al-Zn, which leads to higher current efficiency. However, it might also provide an overlarge anti-corrosion current density for CP and make the CP system unstable. The anodic reaction kinetics of Al-3Zn and Al-20Zn were similar, and there was no evident pitting potential in any case, which indicates that the binary alloy Al-Zn can be a sacrificial anode with a stable activating reaction regardless of the electrolyte concentration.

2) For specimens with CP in an atmosphere environment, both the shifted potential and exchange current density of the steel increased with the concentration. Although self-corrosion might exist for steel in the high-Cl<sup>-</sup>-concentration environment, the active anodic dissolution of the anode alloy provided enough anti-corrosion current density continuously. For the binary Al-Zn anode, the exposure test result showed they can provide sustained CP for steel through an aquiferous fiber sheet in a moisture environment.

3) When the fiber sheet acts as an electrolyte carrier with enough electrolyte inside, the coupling potential of the steel plate is very close to the potential of the anode alloy, regardless of the solution concentration. However, the component contact situation is also influenced by factors such as volume shrinkage of the fiber sheet and deposition of corrosion products. In the actual wet-dry cycles of atmospheric environment, the total area of the exposed holes directly determined the effective CP time. In addition, the high chloride or nonuniform electrolyte is the reason for the occurrence of self-corrosion in the steel plate; they can be avoided by adjusting the dimensions of the exposed holes. Steel with CP system is also under the risk of differential aeration corrosion, which needs to be studied in the future.

#### ACKNOWLEDGMENTS

This work was kindly supported by JSPS KAKENHI Grant Numbers JP19H02227 and JP19K15074. The authors would like to thank Prof. W. Oshikawa from the University of the Ryukyus for his kind help concerning the atmospheric exposure tests and thank Mr. T. Sumitani from Japan Exlan Co., Ltd. for his contributions to the development work about the property study of fiber sheets in this paper. The authors are also grateful to Y. Tsuchihashi from Shutoko Metropolitan Expressway Co., Ltd. and H. Fujimoto from Metawater Co., Ltd., for helping with the indoor exposure test and the atmospheric exposure test during their Master's course internship in Kyushu University.



## STATEMENT

All data included in this study are available upon request by contact with the corresponding author.

## References

1. D. de la Fuente, I. Díaz, J. Simancas, B. Chico, and M. Morcillo, *Corros. Sci.*, 53 (2011) 604.
2. Kainuma S., Mashimoto G., Yang M., and Sajima T., *Zairyo-to-Kankyo*, 67 (2018) 432.
3. T. Tezdogan and Y. K. Demirel, *Brodogradnja : Teorija i praksa brodogradnje i pomorske tehnike*, 65 (2014) 49.
4. R. E. Melchers, in *Condition Assessment of Aged Structures*, Woodhead Publishing Series in Civil and Structural Engineering., 77–106, Woodhead Publishing (2008).
5. Y. Ma, Y. Li, and F. Wang, *Corros. Sci.*, 51 (2009) 997.
6. Y. Ma, Y. Li, and F. Wang, *Corros. Sci.*, 52 (2010) 1796.
7. M. Natesan, G. Venkatachari, and N. Palaniswamy, *Corros. Sci.*, 48 (2006) 3584.
8. G. K. Glass, A. M. Hassanein, and N. R. Buenfeld, *Corros. Sci.*, 43 (2001) 1111.
9. L. Bertolini, M. Gastaldi, M. Pedferri, and E. Redaelli, *Corros. Sci.*, 44 (2002) 1497.
10. L. Bertolini and E. Redaelli, *Corros. Sci.*, 51 (2009) 2218.
11. J. Ma and J. Wen, *J Alloys Compd.*, 496 (2010) 110.
12. J. C. Norris, J. D. Scantlebury, M. R. Alexander, C. J. Blomfield, and R. F. Crundwell, *Surf. Interface Anal.*, 30 (2000) 1.
13. M. Pourgharibshahi and M. Meratian, *Mater. Corros.*, 65 (2014) 1188.
14. R. Orozco-Cruz, J. Genesca, and J. A. Juarez-Islas, in *Corrosion Behaviour and Protection of Copper and Aluminium Alloys in Seawater*, (2007) 159.
15. Z. Marsh, J. Marsch and J. D. Scantlebury, *Journal of Corrosion Science and Engineering*, 2 (1999) 36.
16. S. Szabó and I. Bakos, *Corros. Rev.*, 24 (2006) 231.
17. S. Kainuma, K. Utsunomiya, S. Ishihara, D. Uchida, A. Kaneko, *Zairyo-to-Kankyo*, 60 (2011) 535.
18. C. B. Breslin and W. M. Carroll, *Corros. Sci.*, 34 (1993) 327.
19. D. R. Salinas, S. G. García, and J. B. Bessone, *Journal of Applied Electrochemistry*, 29 (1999) 1063.
20. W. Xiong, G. T. Qi, X. P. Guo, and Z. L. Lu, *Corros. Sci.*, 53 (2011) 1298.
21. Y. Tsuchihashi et al., in Incheon, Korea (2015).
22. S. Kainuma, K. Utsunomiya, S. Ishihara, D. Uchida, A. Kaneko, T. Yamauchi, *Zairyo-to-Kankyo*, 62 (2013) 278.
23. S. Kainuma, Y. Tsuchihashi, S. Ishihara, D. Uchida, A. Kaneko, T. Yamauchi, *Zairyo-to-Kankyo*, 65 (2016) 390.
24. S. Ishihara, S. Kainuma, M. Kinoshita, D. Uchida, A. Kaneko, T. Yamauchi, *Zairyo-to-Kankyo*, 63 (2014) 609.
25. S. Kainuma, M. Yang, S. Ishihara, A. Kaneko, T. Yamauchi, *Constr Build Mater.* (U.R.)
26. JIS G 0579: Method of anodic polarization curves measurement for stainless steels (2007).
27. JIS R 2205: Testing method for apparent porosity, water absorption. specific gravity of refractory bricks (1992).
28. S. L. Wolfson, *Materials Performance*, 33 (1994) 2.
29. C. F. Schrieber and R. W. Murray, *Materials Performance*, 27 (1988) 7.
30. F. Sato and R. C. Newman, *CORROSION*, 54 (1999) 12.
31. T. Ishihara, *The Current Issue Case Histories in Corrosion Failures Analysis and Corrosion Diagnostics*, (2017) Tokyo, Japan.
32. S. Tamari, *J. Soc. Mat. Sci., Japan*, 36 (1987) 636.
33. S. Kainuma, M. Yang, S. Ishihara, A. Kaneko and T. Yamauchi, *Construction Building Materials*,

n.d.

34. S. Kainuma, Y. Tsuchihashi, S. Ishihara, D. Uchida, A. Kaneko and T. Yamauchi, *Journal of Japan Society of Civil Engineers, Ser. A1*, 73 (2017) 2.

© 2019 The Authors. Published by ESG ([www.electrochemsci.org](http://www.electrochemsci.org)). This article is an open access article distributed under the terms and conditions of the Creative Commons Attribution license (<http://creativecommons.org/licenses/by/4.0/>).